Electronic Supplementary Material (ESI) for Lab on a Chip.

A Microfluidic Impedance Platform for Real-Time, *In Vitro* Characterization of Endothelial Cells Undergoing Fluid Shear Stress

Supplementary Material

Fabrication process

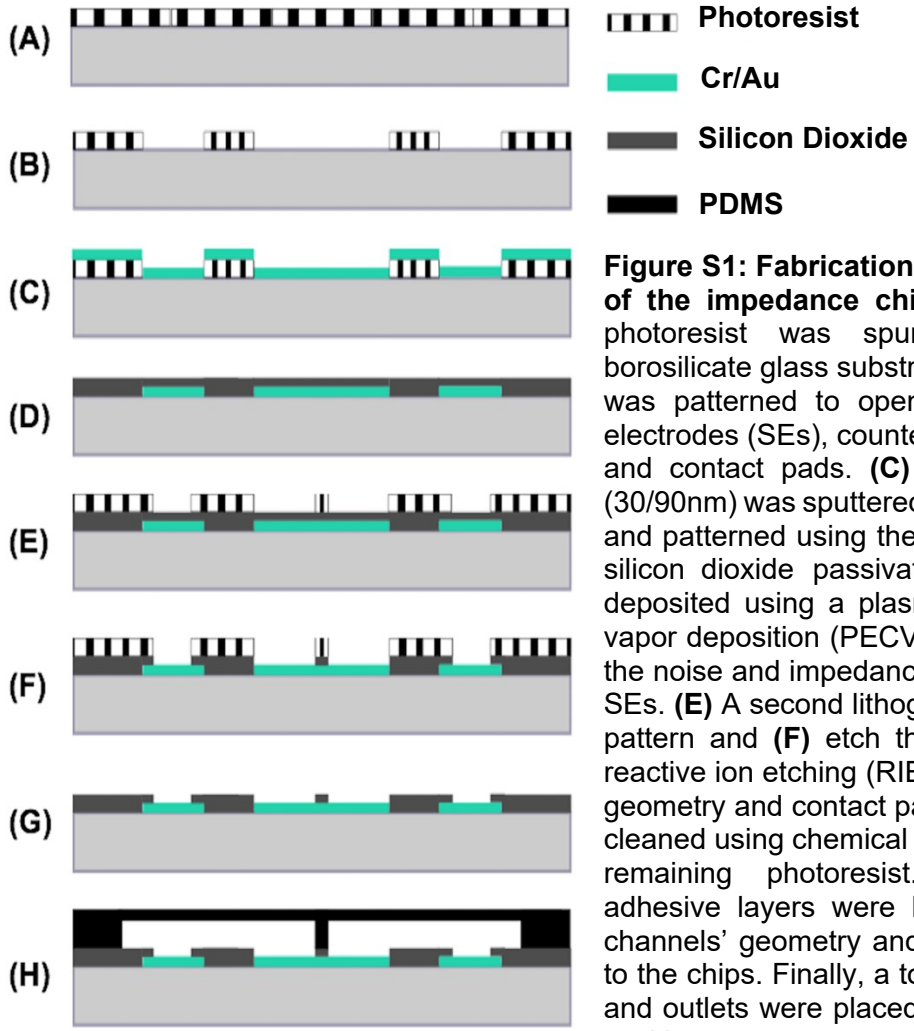

Figure S1: Fabrication process flow diagram of the impedance chip. **(A)** A thin layer of photoresist was spun on 4-inch square borosilicate glass substrate. **(B)** The photoresist was patterned to open windows for sensing electrodes (SEs), counter electrode (CE), wires, and contact pads. **(C)** A thin layer of Cr/Au (30/90nm) was sputtered on to borosilicate glass and patterned using the lift-off technique. **(D)** A silicon dioxide passivation layer (1 μm) was deposited using a plasma enhanced chemical vapor deposition (PECVD) to electrically isolate the noise and impedance not contributed by the SEs. **(E)** A second lithography step was used to pattern and **(F)** etch the silicon dioxide using reactive ion etching (RIE) to define the SEs, CE geometry and contact pads. **(G)** The chips were cleaned using chemical solvents to dissolve any remaining photoresist. **(H)** Double sided adhesive layers were laser cut to define the channels' geometry and subsequently adhered to the chips. Finally, a top PDMS lids with inlets and outlets were placed on top to seal channel cavities.

Chip Characterization

Initial characterization on electrode size based behavior and solution conductivity were performed with biologically relevant electrolyte solutions to determine behavior and sensitivity of microelectrodes. These different conductivity solutions consisted of: deionized (DI) water, potassium chloride (KCl), 1X phosphate buffered saline (PBS), and cell culture medium (Medium 200, Life Technologies, Carlsbad, CA; Cat No. M-200-500) (Fig. S2D). These experiments were

carried out at ambient conditions. Measurements were initiated with the least conductive solution and continued incrementally to the most conductive solutions. Devices were rinsed three times with DI water between solution measurements. Before each acquisition, fifteen minutes were allotted for the solution to reach steady state with the electrodes.

Electrode Size Effect

Impedance magnitude increased with decreasing electrode surface area (Fig. S2A-C). The CPE slope and the R_{MED} plateau were derived at higher impedance magnitudes as the electrode diameter decreases. In addition, the resistive component (R_{MED}) was observed at a higher frequency values with decreasing electrode geometry, as documented in other works [1]. As the electrode diameter decreased, the frequency independent region became narrower, where the 50 µm diameter electrodes displayed no notable resistance plateau and the behavior resembled that of capacitive charging. In conjunction, the complementary phase plots (Fig. S3A-C) showed that with decreasing electrode size, the phase shift values were recorded closer to -90°, which is also indicative of capacitive behavior. As a result, this data confirmed that for the 50 µm electrodes, the interfacial impedance dominated measurements making them inaccurate for R_{TER} cellular measurements.

Solution Conductivity Effect

Solution conductivity effects on impedance spectra were also explored in the data presented in Fig. S2. As the solution conductivity increased, the resistance plateau in the impedance magnitude plots shifted down. Simultaneously, the phase shifts curves moved to higher frequencies with increased solution conductivity. This behavior followed the inverse relationship between solution resistance and conductivity for two electrodes in series[2].

Additionally, phase shift plots portrayed slightly higher amplitudes for higher conductivity solutions KCl D and KCl E but not for the cell culture media. Despite having a higher conductivity, cell culture media's phase shift has a similar amplitude as KCl A, B, and C. This behavior observed may be attributed to the complex composition of cell culture media compared to a simple binary electrolyte solution like KCl.

Fluid Flow Effects

The impedance platform was tested to measure the effects of fluid flow on impedance measurement (Fig. S3). Past published studies involving impedance spectra of cells under flow neglected to explore flow effects and determine if it was needed to isolate them from the data related to actual cell behavior[3–5]. For these studies, chips were tested with three different solutions: KCl M, PBS, and cell culture media. Both KCl M and PBS were adjusted to be of similar conductivity values as medium (Fig. S3D). Fig. S3A-C show normalized plots of impedance magnitude ($|Z|_{flow}/|Z|_{static}$) and phase shift ($\theta_{flow}/\theta_{static}$) as a function of frequency for the solutions mentioned above and fluid flow condition was set at the constant shear value, 17.6 dyne/cm^2.

Fluid flow generated an increase in $|Z|$ only for KCl M (not PBS or media) at the frequency range 100 -100,000 Hz, where the $|Z|$ increase quantity was electrode-size dependent. Under flow conditions, impedance magnitude ($|Z|$) at 1 kHz was measured 38%, 25%, and 10% higher than static measurements for the 200, 100, and 50 µm SEs, respectively. As the electrode diameter decreased, fluid flow effects were less distinguishable due to reduced electrode sensitivity.

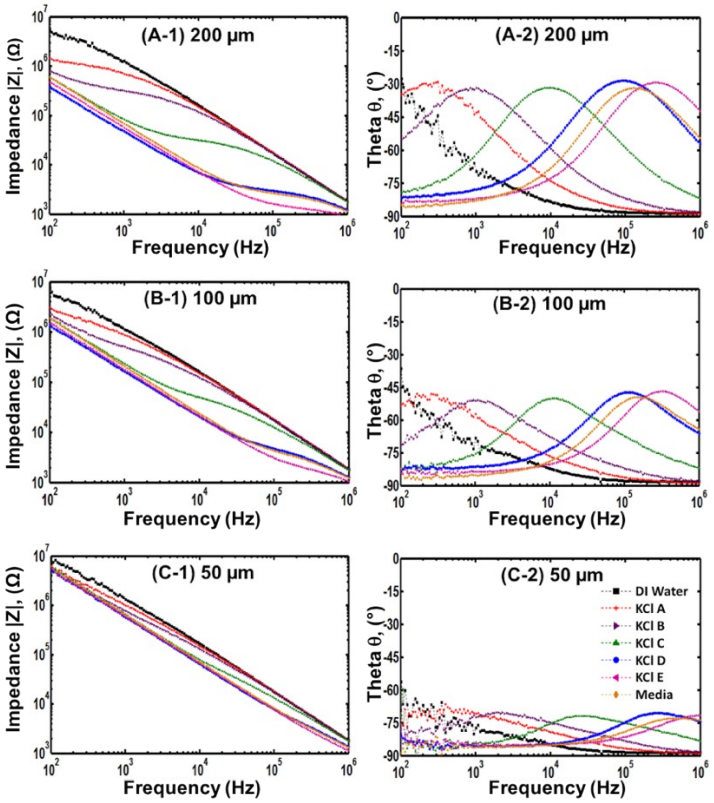

D Symbol	Solution	Conductivity, σ (mS/cm)
■	DI Water	0.006
✱	KCl A	0.0243
▶	KCl B	0.203
▲	KCl C	2.16
●	KCl D	24.7
◀	KCl E	59.1
◆	Media	27

Figure S2: Bode plots for **(A)** 200 µm, **(B)** 100 µm and **(C)** 50 µm electrodes measuring different **(D)** conductivity solutions: DI water KCl A, KCl B, KCl C, KCl D, KCl E, and Media.

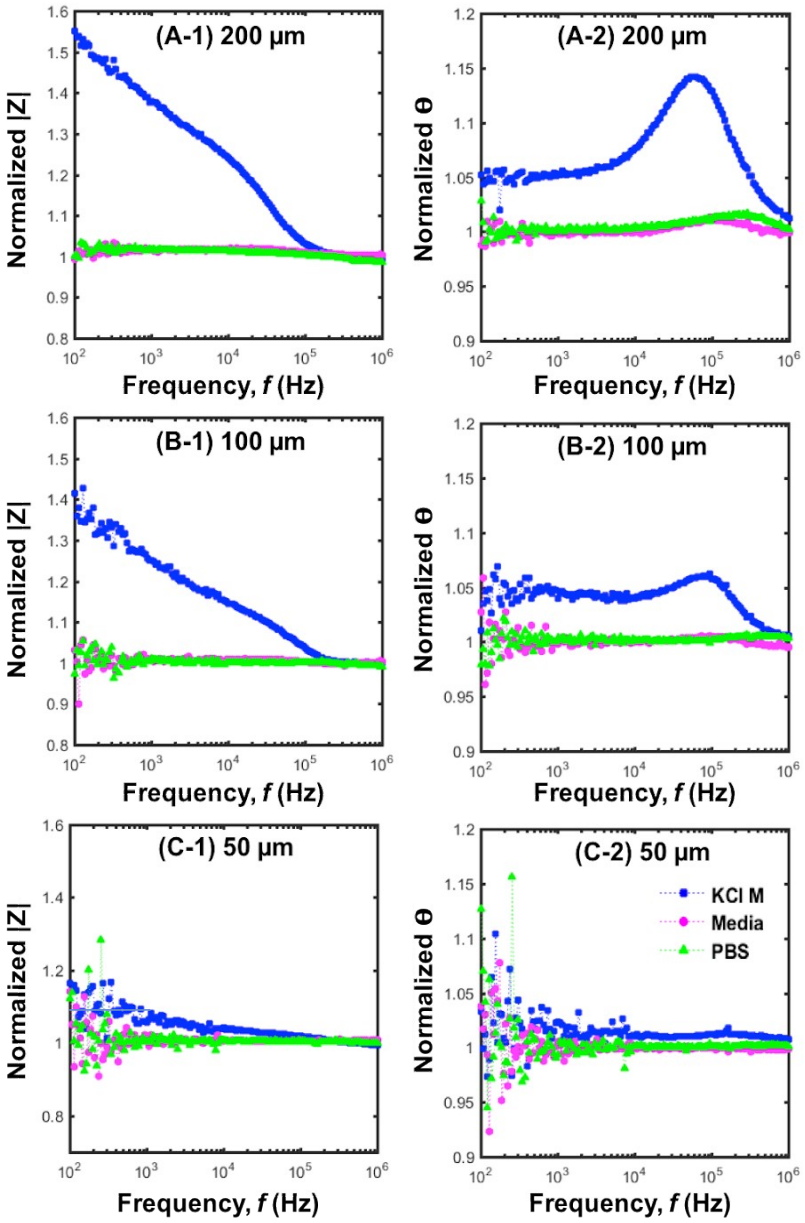

D Symbol	Solution	Conductivity, σ (mS/cm)
■	KCl M	27.2
●	Media	27
▲	PBS	27.1

Figure S3: Normalized measurements ($|Z|_{flow}/|Z|_{static}$ and $\theta_{flow}/\theta_{static}$) of impedance magnitude and phase shift for **(A)** 200 µm, **(B)** 100 µm and **(C)** 50 µm diameter electrodes. The normalized values were calculated as ratio of the measurements collected under flow (17.6 dyne/cm^2) to static conditions for **(D)** different solutions: KCl M, Media, and PBS.

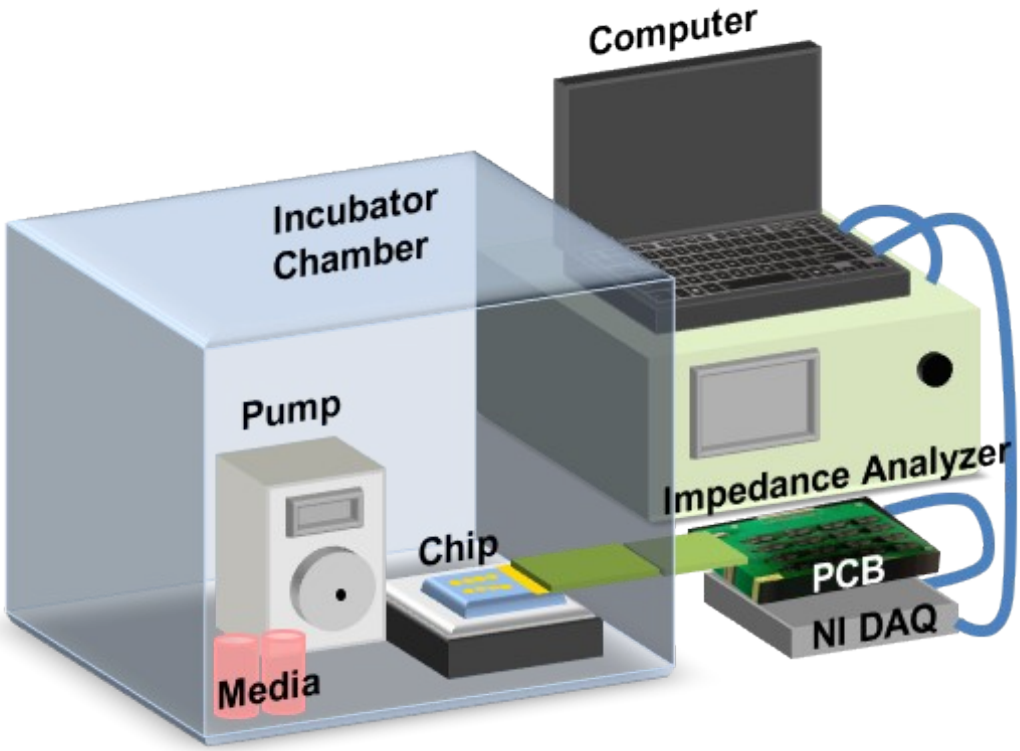

Figure S4: Illustration of the microfluidic impedance platform and experimental set-up. The microfluidic impedance chip was connected via a card reader to a custom printed circuit board designed to automatically collect impedance spectra from an impedance analyzer (100 Hz-1 MHz) and store the acquired data in a portable computer. The chip was also coupled to medium reservoirs and a peristaltic pump which subjected cells to shear stresses. The chip, pump, and medium reservoirs were maintained in an incubator chamber with controlled temperature and humidity settings during experimentation.

Equivalent Circuit Components

Constant Phase Element (CPE)

The CPE is the non-ideal capacitance at the liquid-electrode interface due to charge accumulation once the potential is applied. Although, this electric double layer is usually modeled as a parallel plate capacitor, electrode surface roughness and porosity, passivation composition, plus, non-uniform potential and current distributions create deviations from an ideal capacitor behavior[2,6]. This non-ideal capacitance behavior is better accounted for by the impedance of CPE:

$$Z_{CPE} = \frac{1}{Y(j2\pi f)^n}$$

Where *f* is the frequency value, *Y* is a constant describing the magnitude of CPE and is equivalent to an ideal capacitance, and *n* is a power factor ranging between 0 and 1 which can be used to describe the phase angle as -90**n.* The *n* parameter accounts for the non-

linear impedance of the electric double layer on the gold surface. When n=1, the impedance of the CPE is equal that of an ideal capacitor, if n=0, the impedance of CPE is that of an ideal resistor.

Image Analysis

VE-Cadherin Analysis

To initiate the analysis, the DAPI and VE-Cadherin images of tested samples were processed using a Gaussian Blur filter in order to smoothen clusters of fluorescent pixels. This step enabled the ability to capture thin lines of expressed VE-Cadherin that would go unrecognized by the software if otherwise. Once pixels were smoothed out, images were converted to binary format. The binary images of DAPI images were subtracted from the VE-Cadherin images to eliminate any DAPI fluorescence in the VE-Cadherin images. Subtracted images were inspected and if any nuclei signal remained, these were manually removed. Then, using the ellipse tool, the specified area of analysis (electrode area) was defined. The “Analyze Particles” command was selected to measure the binary images of VE-Cadherin. This command basically scans the selected area until it detects the edge of VE-Cadherin junctions. Using the wand tool, this command outlines the VE-Cadherin junction and measures the area, grey value and integrated density value of selected pixels. Next, it fills measured object to make it undetectable until it completes processing the entire selected electrode area.

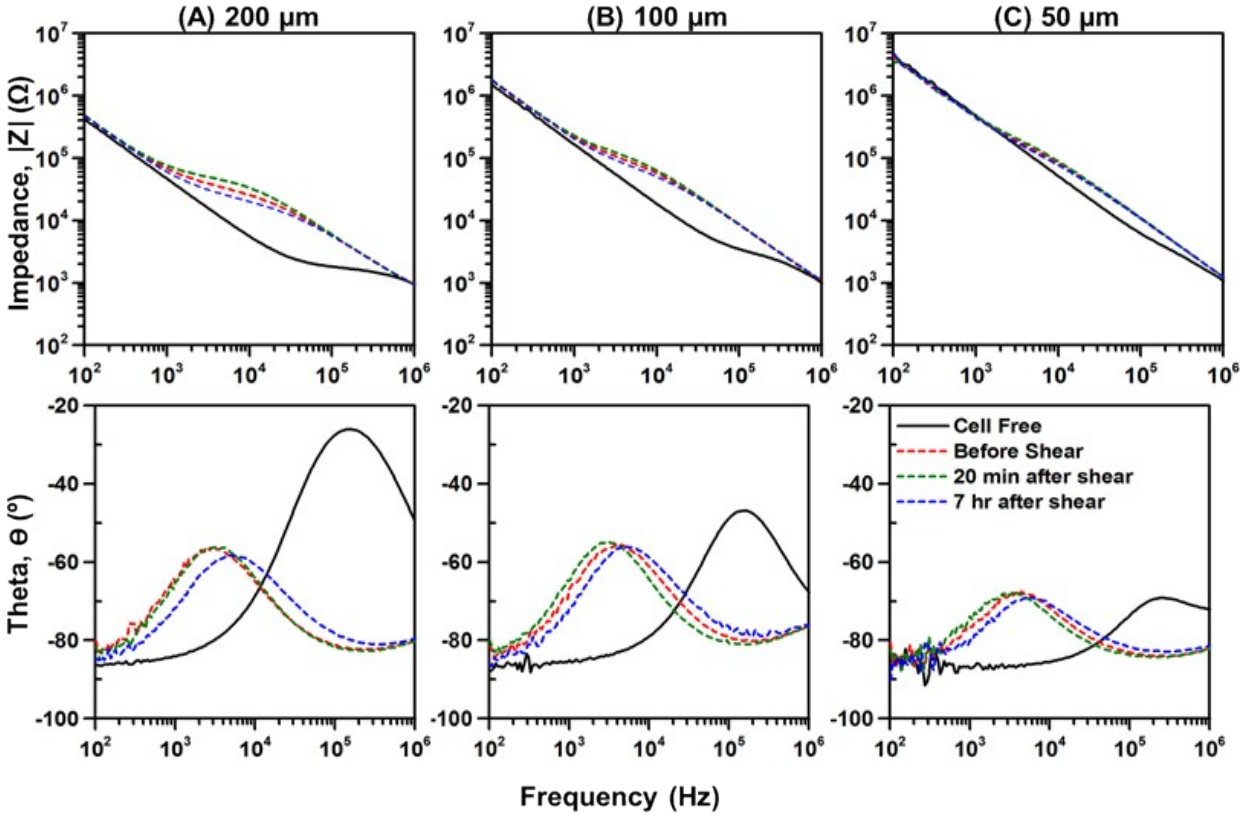

Figure S5: Bode plots for **(A)** 200 µm, **(B)** 100 µm, and **(C)** 50 µm electrodes for cell free control, HUVECs under static condition, HUVECs sheared (17.6 dyne/cm^2) after 20 min, and after 7 hours.

	Shear Conditions (dyne/cm^2)	Initial Jump, ↑BV (time)	Falls under static	Minimum, ↓BV (time)	End Value
$R_{TER, 200}$	0	XX		26%	22%
	17.6	24% (24 min)	2.8 hr	38% (~6hr)	28%
	23.7- 35- 58.1	42% (48 min)	5.6 hr	31% (~8.4hr)	5%
$R_{TER, 100}$	Static	XX		40% (~4.4hr)	31%
	17.6	15% (24 min)	9hr	35% (~13hr)	33%
	23.7- 35- 58.1	36% (72 min)	6 hr	50% (~10hr)	19%

Table S1: Table showing the features of normalized R_{TER} where BV stands for baseline value.

References

1 A. Ahuja and M. Behrend, *IEEE Trans. Biomed. Eng.*, 2008, **55**, 1457–1460.

2 D. Price, A. Rahman and S. Bhansali, *Biosens. Bioelectron.*, 2008, **24**, 2071–6.

3 N. DePaola, J. E. Phelps, L. Florez, C. R. Keese, F. L. Minnear, I. Giaever and P. Vincent, *Ann. Biomed. Eng.*, 2001, **29**, 648–656.

4 J. Seebach, P. Dieterich and F. Luo, *Lab. …*, 2000, **80**, 1819–31.

5 J. Seebach, G. Donnert, R. Kronstein, S. Werth, B. Wojciak-Stothard, D. Falzarano, C. Mrowietz, S. W. Hell and H. J. Schnittler, *Cardiovasc. Res.*, 2007, **75**, 596–607.

6 A. Rahman, C. Lo and S. Bhansali, *IEEE Trans. Biomed. Eng.*